Journal of the European Ceramic Society **14** (1994) 473–479

An Initial Stage Model for the Sintering of Constrained Polycrystalline Thin Films

Douglas R. Carroll*[a] & Mohamed N. Rahaman[b]

[a] Basic Engineering Department, [b] Ceramic Engineering Department, University of Missouri-Rolla, Rolla, Missouri 65401, USA

(Received 13 July 1993; revised version received 15 April 1994; accepted 27 May 1994)

Abstract

A physical model has been developed for the initial stage of sintering of thin constrained polycrystalline films. The model compares the shrinkage of constrained thin films to the shrinkage of unconstrained or free sintering material. It predicts that the volumetric shrinkage of a constrained thin film will be slightly more than the linear shrinkage for the free sintering case, but far less than the volumetric shrinkage for the free sintering case. Model predictions show that the sintering of a constrained film is highly dependent on the ratio of the boundary energy to the surface energy, and on grain growth. The model was used to fit the experimental data of Garino & Bowen, for the sintering of constrained alumina and zinc oxide films (Garino, T. & Bowen, H. K., *J. Am. Ceram. Soc.*, **70**(9) (1987) C210–211).

Ein physikalisches Modell für die erste Phase beim Sintern von dünnen, gebundenen, polykristallinen Filmen wurde entwickelt. Mit Hilfe des Modells wurde die Schrumpfung dünner, gebundener Filme mit der Schrumpfung nicht gebundener Filme oder frei gesintertem Material verglichen. Das Modell sagt voraus, daß die volumetrische Schrumpfung eines dünnen, gebundenen Films etwas größer ist als die lineare Schrumpfung im Falle frei gesinterter Proben, aber weit weniger stark als die volumetrische Schrumpfung frei gesinterter Proben. Die Modellberechnungen zeigen, daß das Sintern eines gebundenen Films in starkem Maße vom Verhältnis der Grenzflächenenergie zur Oberflächenenergie und vom Kornwachs tum abhängt. Die Modellrechnungen wurden mit den experimentellen Daten von Garino und Bowen für das Sintern von gebundenem Aluminiumoxid und Zinkoxidfilm verglichen (Garino, T. & Bowen, H. K., *J. Am. Ceram. Soc.*, **70**(9) (1987) C210–211).

* To whom correspondence should be addressed.

Un modèle physique a été développé pour l'étape initiale du frittage de films minces polycristallins sous contrainte. Le modèle compare le retrait d'un film mince sous contrainte à celui d'un matériau sans contrainte ou fritté sans charge. Ce modéle prévoit que le retrait volumique d'un film mince sous contrainte sera légèrement supérieur au retrait linéaire dans le cas d'un frittage sans charge mais très inférieur au retrait volumique dû au frittage sans charge. Les prédictions du modèle montrent que le frittage d'un film sous contrainte est fortement dépendant du rapport entre l'énergie des joints et l'énergie de surface et de la croissance des grains. Le modèle a été utilisé pour lisser les données expérimentales de Garino et Bowen pour le frittage de films d'alumine et d'oxyde de zinc sous contrainte (Garino, T. & Bowen, H. K., *J. Am. Ceram. Soc.*, **70**(9) (1987) C210–11).

1 Introduction

The sintering of thin ceramic films is of both theoretical and practical interest. Thin films are used for magnetic recording devices, wear-resistant coatings, high-temperature coatings, optical films and in many areas of electronics. This paper focuses on the development of a theoretical model which is suitable for the sintering of thin polycrystalline films.

Two models have been developed for the sintering of constrained films. A common feature of these models is that the body is assumed to be a viscous continuum. Scherer & Garino[1] used a cubic cylinder model, which was an extension of previous work by Scherer.[2,3] The cubic array of cylinders was used to establish the kinetics for the model, but for the kinematics the material was assumed to be a viscous continuum in which the normal viscosity and Poisson's ratio varied with the relative density. Bordia & Raj[4] modeled the thin film as a linear viscoelastic solid with spherical

Journal of the European Ceramic Society 0955-2219/94/$7.00

isolated pores. Neither model accurately represents the sintering of thin polycrystalline films.

Two important reasons may be put forward to explain why continuum models are inadequate to represent the sintering of polycrystalline films. Firstly, the kinematics associated with continuum models is not at all similar to the kinematics of a sintering process governed primarily by diffusion processes which are directionally specific. Secondly, continuum models neglect grain boundaries and grain growth phenomena, which is equivalent to putting the grain boundary energy equal to zero. This is a serious limitation, since the grain boundary energy in ceramic materials can be comparable to the surface energy.

For this work, a model in which the kinematics more closely resemble those of grain boundary and surface diffusion was developed. It is similar to the two sphere model by Johnson,[5] except the geometry has been specialized for the case of a constrained thin film.

2 Sintering Geometry

The model assumes that all densification occurs through neck growth. It is assumed that the material is made up of spherical particles stacked in a simple cubic array as shown in Fig. 1, and that the densification occurs at constant temperature. As the material densifies, necks form between the spheres, and the centers of the spheres get closer together. If the material is unconstrained, then the centers of the spheres get closer together in all three coordinate directions. If the material is a constrained thin film, then the spheres can get closer together only in the thickness (z) direction.

2.1 Free sintering case

To explain the details of the model it is convenient to work with a quarter circle. Figure 2 shows the parameters used in modeling the free sintering, and the sintering of constrained thin films. For the free sintering case, there will be penetration on all six sides of the spherical particle, and all of the necks will have the geometry depicted as the top neck in Fig. 2. The symbol ρ is the sphere radius. V_R represents the volume of material removed from the sphere, due to penetration, and placed in the neck region. If the top shaded area labeled V_R is revolved around the y-axis, the volume generated is the volume removed. If the top shaded area labeled V_1 is revolved around the y-axis, the volume generated is the volume of the neck. The symbol ϕ is the angle associated with the volume removed, ψ is the angle associated with the neck, α is half the dihedral angle, and γ, r, s and β are as shown in the figure. It is reasonable to assume that the density of the solid material is constant, since the temperature is constant and no external forces are applied, thus conservation of mass requires that the volume of solid material be conserved, i.e.

$$V_R = V_1 \tag{1}$$

The volumes V_R and V_1 can be expressed in terms of the other parameters. In addition to this there are some obvious geometric relations, and the following equations can easily be derived:

$$V_R = \frac{4\pi}{3}\rho^3 \sin^2\left(\frac{\phi}{2}\right) - \frac{\pi}{3}\rho^3 \sin^2\phi\cos\phi \tag{2}$$

$$\begin{aligned} V_1 = {} & \frac{\pi}{3}(\rho + r)^3 \cos(\phi + \psi)\sin^2(\phi + \psi) \\ & - \frac{\pi}{3}\rho^3 \cos\phi \sin^2\phi \\ & - \frac{4\pi}{3}\rho^3 \sin\left(\frac{\psi}{2}\right)\sin\left(\phi + \frac{\psi}{2}\right) \\ & - \pi\beta(\rho + r + s)(r + s)^2 \sin(\phi + \psi) \\ & + \pi(\rho + r + s)(r + s)^2 \sin(\phi + \psi) \\ & \cos(\gamma - \beta)\sin(\gamma - \beta) \\ & - \frac{\pi}{3}(r + s)^3 \cos^2(\gamma - \beta)\sin(\gamma - \beta) \\ & + \frac{\pi}{3}s^3 \cos^2\gamma \sin\gamma \\ & + \frac{4\pi}{3}(r + s)^3 \sin\left(\frac{\beta}{2}\right)\cos\left(r + \frac{\beta}{2}\right) \\ & - \pi(\rho + r + s)s^2 \sin(\phi + \psi)\sin\gamma\cos\gamma \end{aligned} \tag{3}$$

$$\rho\cos\phi = (\rho + r)\cos(\phi + \psi) \tag{4}$$

$$\gamma + \phi + \psi = \frac{\pi}{2} \tag{5}$$

$$\beta = \gamma + \alpha - \frac{\pi}{2} \tag{6}$$

$$s\sin\gamma = (r + s)\sin(\gamma - \beta) \tag{7}$$

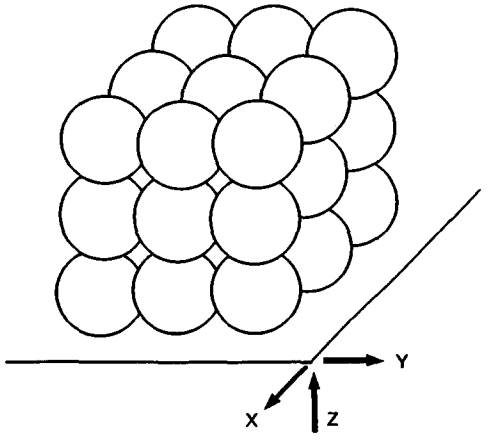

Fig. 1. Spherical particles stacked in a simple cubic array.

Equations (1) to (7) establish the geometry of the model. After the dimensioned parameters are normalized with respect to ρ, the eight variables are V_R/ρ^3 V_1/ρ^3, r/ρ, s/ρ, ϕ, ψ, γ and β. It is mathematically most convenient to work in terms of the angle ϕ thus it can be said that, given ϕ, eqns (1) to (7) specify a unique solution for the other seven variables.

2.2 Constrained thin film case

In modeling the sintering of constrained thin films, it was assumed that the spheres could not get closer together in the x and y directions, as illustrated in Fig. 1. Volume will be removed from the top and bottom of the spheres but not from the sides. Assuming the density of the material remains constant and applying conservation of volume as in the free sintering case, it follows that the volume removed from the top and bottom is equal to the volume placed in the necks. Parameters for the top and bottom necks are the same as for the free sintering case. The volume of material in each of the side necks is V_2, θ is the angle associated with the side neck, and r_2, s_2, γ_2 and β_2 are as shown in the figure. Conservation of mass requires:

$$2V_R = 2V_1 + 4V_2 \tag{8}$$

and the following equations can be derived from the geometry.

$$\begin{aligned} V_2 = {} & \frac{\pi}{3}(\rho + r_2)^3 \sin^2\theta \cos\theta - \frac{4\pi}{3}\rho^3 \sin^2\left(\frac{\theta}{2}\right) \\ & + \pi(\rho + r_2 + s_2)(r_2 + s_2)^2 \sin\theta \\ & \cos(\gamma_2 - \beta_2)\sin(\gamma_2 - \beta_2) \\ & - \frac{\pi}{3}(r_2 + s_2)^3 \cos^2(\gamma_2 - \beta_2)\sin(\gamma_2 - \beta_2) \\ & - \pi\beta_2(\rho + r_2 + s_2)(r_2 + s_2)^2 \sin\theta \\ & - \pi(\rho + r_2 + s_2)s_2^2 \sin^2\theta\cos\theta \\ & + \frac{4\pi}{3}(r_2 + s_2)^3 \sin\left(\theta + \frac{\beta_2}{2}\right)\sin\left(\frac{\beta_2}{2}\right) \\ & + \frac{\pi}{3}s_2^3 \sin^2\theta\cos\theta \end{aligned} \tag{9}$$

$$\rho = (\rho + r_2)\cos\theta \tag{10}$$

$$\gamma_2 + \theta = \frac{\pi}{2} \tag{11}$$

$$\alpha + \gamma_2 - \beta_2 = \frac{\pi}{2} \tag{12}$$

$$s_2 \sin\gamma_2 = (r_2 + s_2)\sin(\gamma_2 - \beta_2) \tag{13}$$

Equations (2) to (13) can be normalized with respect to the sphere radius ρ, generating 12 equations with 14 variables V_R/ρ^3, V_1/ρ^3, V_2/ρ^3, r/ρ, s/ρ, r_2/ρ, s_2/ρ, ϕ, ψ, β, γ, θ, β_2 and γ_2. One more relation must be specified in order to completely define the geometry. It must be decided how much of the removed volume goes into the top and bottom necks and how much goes into the side necks.

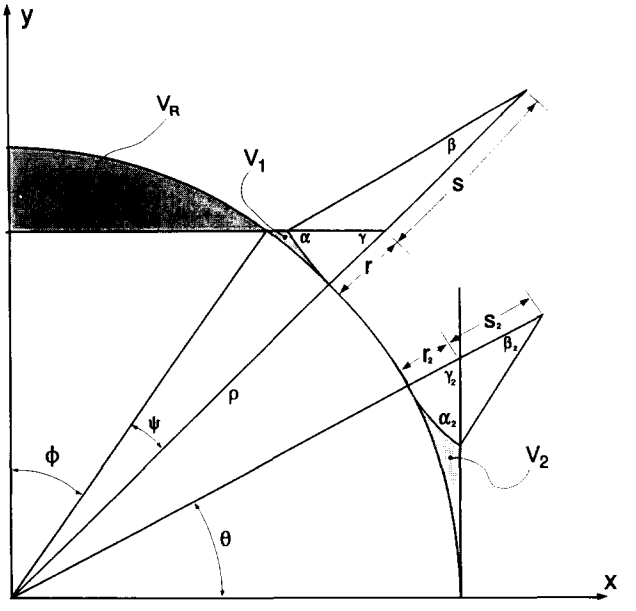

Fig. 2. Parameters used in modeling the sintering.

For the assumed spherical geometry of the particle, there is no chemical potential to cause material to flow from the top and bottom necks, around and into the side necks, because the curvature of a sphere is constant. Therefore, it could be assumed that none of the material removed from the top and bottom of the sphere goes into the side necks. Material could flow from the surface of the spheres into the side necks by surface diffusion, but surface diffusion is not a densifying mechanism. Under this assumption, the relative density or shrinkage of the constrained thin film would be independent of what happens in forming the side necks. Densification would be governed by the kinetics of forming the top and bottom necks. Thus if it is assumed that none of the material removed from the top and bottom of the sphere goes into the side necks, then the volumetric shrinkage of the constrained thin film would be exactly equal to the linear shrinkage for the free sintering case.

Assuming that none of the material removed from the top and bottom of the spheres flows into the side necks is in reasonably good agreement with experimental data for ZnO and Al_2O_3 constrained films from Garino and Bowen.[6] However, careful examination of the data shows that the volumetric shrinkage of the constrained film ranged from slightly more than the linear shrinkage for the free sintering case, to 50% more than the linear shrinkage for the free sintering case. Therefore, assuming that none of the material removed from the top and bottom flows into the

side necks gives a low estimate for the shrinkage of the constrained thin films, because it assumes the densification is independent of what happens in the side necks. At some point in the process, the side necks will begin to act as material sinks, drawing material from the top and bottom necks into the side necks.

Early in the densification process, material will flow from the surface of the sphere into the side necks by surface diffusion. The spheres will become non-spherical, and there will be a gradient in the curvature of the spheres, with the curvature being higher close to the side necks. This gradient in the curvature will progress around the spheres until it intersects the top and bottom necks, and provides the chemical potential for material to flow from the top and bottom necks into the side necks by surface diffusion. This explanation is in better agreement with the experimental data[6] for the ZnO and Al_2O_3 constrained films. Early in the densification process, the volumetric shrinkage of the constrained film was slightly more than the linear shrinkage for the free sintering case, and this could be explained from the model, since the gradient in the curvature had not yet intersected the top and bottom necks. Later in the densification process, the volumetric shrinkage for the constrained film was significantly more than the linear shrinkage for the free sintering case, and this could be explained from the model by saying that the gradient in the curvature had reached the top and bottom necks, and the side necks were acting as material sinks, enhancing the densification of the thin film. The assumed geometry is an approximation which includes the most important aspects of the initial stage of the sintering process. Material is removed from the top and bottom of the spheres and placed in the top and bottom necks, and some of the material is transported to the side necks.

The most reasonable way to control how much material goes into the top and bottom necks, and how much goes into the side necks, is to define a ratio between the top and bottom neck parameter r and the side neck parameter r_2. If $r_2 = 0$, then all of the material is placed in the top and bottom necks, while if $r = 0$, all of the material is placed in the side necks. Several ratios were tried in developing the model. Figure 3 shows a comparison of five cases, assuming the dihedral angle was 150°, no grain growth, and using the kinetics developed later in the paper. Placing all the material in the side necks gave the most shrinkage (but is physically unrealistic), and placing all the material in the top and bottom necks gave the least shrinkage. The center curve was generated by setting $r = r_2$, and the curves just above and below it were

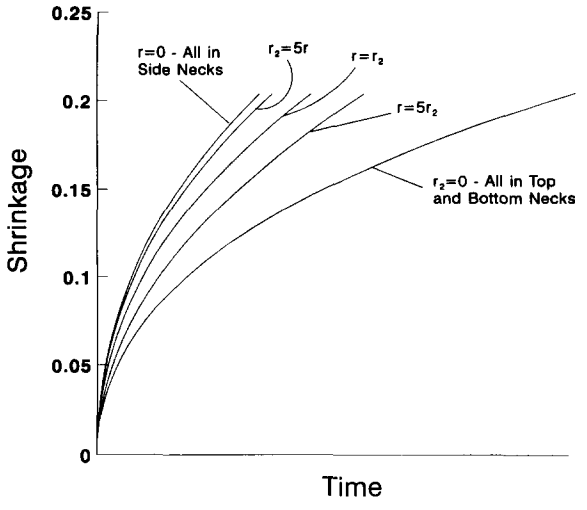

Fig. 3. Effect of placing material in the top and bottom, or side necks.

generated by setting $r_2 = 5r$ and $r = 5r_2$, respectively. From this comparison it can be seen that the ratio chosen to relate r to r_2 does not dramatically effect the results of the model, so it was decided that setting $r = r_2$ was the most reasonable assumption.

3 Kinetics

The kinetics for these geometries can be derived from the basic atomic flux equation, using the procedure outlined by Johnson.[5] Defining B_a, as the atomic mobility, C_a as the concentration and μ_a as the chemical potential, the basic atomic flux equation can be written as:

$$j = -B_a C_a \nabla \mu_a \tag{14}$$

Defining Σ as the sintering pressure and Ω as the atomic volume, $C_a = 1/\Omega$ and $\nabla \mu_a = \Omega \nabla \Sigma$. Assuming the atomic mobility is constant along the grain boundary, the flux gradient must also be constant. Making these substitutions in eqn (14), it follows that $\nabla^2 \Sigma$ must be constant. The general solution for Σ is:

$$\Sigma = Q_1 R^2 + Q_2 \ln R + Q_3 \tag{15}$$

where Q_1, Q_2 and Q_3 are constants and R is the radial coordinate. For boundary conditions it was assumed that the sintering pressure was zero at $R = 0$, and a maximum on the surface of the neck. The maximum on the surface Σ_{max} was developed by Raj[7] as:

$$\Sigma_{max} = \left[\frac{\partial I}{\partial V_T}\right]_{V_g} \tag{16}$$

where I is the free energy of the system, V_T is the total volume including the pores and V_g is the volume of solid material. For this model the free

energy was assumed to consist of surface energy and grain boundary energy, and it was assumed that γ_s and γ_b were constant over the surface and grain boundary areas respectively. It was assumed that material was transported along the grain boundary by grain boundary diffusion, and deposited in the neck region. Surface diffusion then rearranged the material into the assumed neck shapes. Surface diffusion was assumed to be much faster than grain boundary diffusion so that the kinetics of the process was governed by the grain boundary diffusion.

Defining D_f as the relative density for the free sintering case, and D_c as the relative density of the constrained film, the following equations were derived:

$$\frac{1}{D_f}\frac{dD_f}{dt} = \frac{3A}{[(\rho + r + s)\sin(\phi + \psi) - (r + s)\cos(\gamma - \beta)]^2 \rho \cos\phi} \left[\frac{\partial I}{\partial V_T}\right]_{V_g} \quad (17)$$

$$\frac{1}{D_c}\frac{dD_c}{dt} = \frac{A}{[(\rho + r + s)\sin(\phi + \psi) - (r + s)\cos(\gamma - \beta)]^2 \rho \cos\phi} \left[\frac{\partial I}{\partial V_T}\right]_{V_g} \quad (18)$$

where A is the product of several terms (atomic diffusion coefficient, grain boundary thickness, atomic volume, Boltzman's constant and temperature). The parameter A is constant at a given temperature, and in practice A was adjusted to best fit the experimental data. It is tempting to say the equations differ only by a factor of 3, but the geometric relationships between the variables in eqn (17) are different from those for eqn (18), so there is a significant, although subtle, difference between the equations. These two equations can be integrated numerically to get the relative density or shrinkage as a function of time.

Grain growth can have a significant effect on the densification rate, as the larger grains absorb the smaller grains. The driving force for grain growth is reduction of the free energy by reducing the grain boundary energy (or area) per unit volume. Increasing the grain size increases the distances over which atomic diffusion must occur for the material to densify, and thus reduces the densification rate. The only way to include grain growth in this model was to allow the spheres to grow uniformly with time. This approximation does not account for the fact that larger grains absorb smaller grains, and the number of grains decreases during the densification process. However, allowing the spheres to grow uniformly does reduce the grain boundary and surface area per unit volume, which reduces the sintering pressure ($\partial I/\partial V_T$) in eqns (17) and (18). As the grain size increases, the distance for grain boundary diffusion increases proportionally, thus the denominator in eqns (17) and (18) varies with the cube of the grain size. Accounting for both the reduction in sintering pressure and the increased distance for atomic diffusion, the densification rate varies inversely with the grain size to the fourth power.

4 Results and Discussion

The dihedral angle has a significant effect on the sintering behavior of the material, as illustrated in Fig. 4. The densification rate for large dihedral angles is much faster than for smaller dihedral angles. Changing the dihedral angle affects the sintering pressure ($\partial I/\partial V_T$), because it changes the ratio γ_b/γ_s. During the densification process, the surface energy decreases, while the grain boundary energy increases, and the sintering pressure is proportional to the difference between these two quantities. For large dihedral angles, the increase in the grain boundary energy is small compared with the reduction in surface energy, because γ_b/γ_s is small. However, for smaller dihedral angles, the increase in grain boundary energy is comparable to the reduction in surface energy, and this significantly reduces the sintering pressure, and slows the densification. This result suggests that experimental studies showing how the dihedral angle of a material varies over a range of possible sintering temperatures, would be helpful in developing a sintering process for the material. Readey & Jech[8] showed that the ratio γ_b/γ_s for nickel oxide varied dramatically with temperature, from 1·05 at

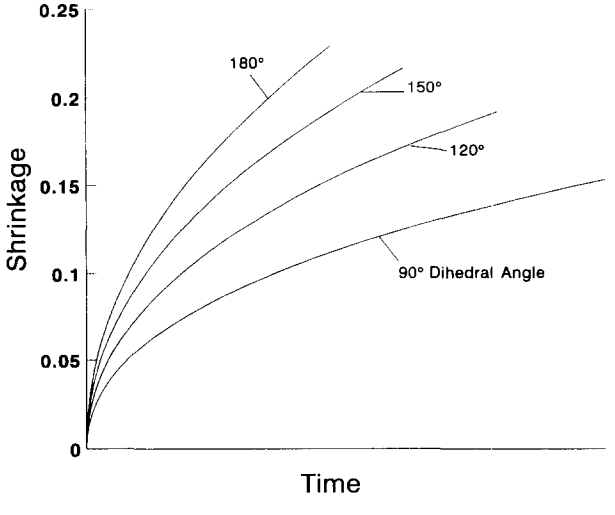

Fig. 4. Effect of dihedral angle on the shrinkage.

1311°C to 0·22 at 1589°C. Nickel oxide is a highly non-stoichiometric material, and is perhaps not typical of other ceramic materials, but the study suggests that the dihedral angle may vary with temperature. Data showing how γ_b/γ_s varies with temperature is not available for other materials.

The model can be compared to experimental data for the sintering of polycrystalline thin films. Garino & Bowen[6] published experimental data for the sintering of constrained and unconstrained films of aluminum oxide, Al_2O_3, and zinc oxide, ZnO. The sintering temperatures for the Al_2O_3 and ZnO were 1285°C and 778°C respectively and the initial relative density of the films was approximately 0·55, which compares well with the value of 0·524 for the present model. The total volumetric shrinkages were 33% and 24% for the unconstrained Al_2O_3 and ZnO films respectively. This would correspond to final relative densities of 82% and 72% for the unconstrained Al_2O_3 and ZnO films respectively, so it is reasonable to expect that an initial stage sintering model would fit this experimental data. In fitting the model predictions to the experimental data, it is necessary to make reasonable estimates for the ratio γ_b/γ_s, and for the grain growth of the material. Handwerker *et al.*[9,10] showed that γ_b/γ_s was between 1·1 and 1·2 for MgO at 1247°C and Al_2O_3 at 1647°C. Based on these experimental studies, it was decided that $\gamma_b/\gamma_s = 1{\cdot}2$ was a reasonable value for the two thin films, and that was the value used in fitting the model to the experimental data. Garino & Bowen reported 29% grain growth for the Al_2O_3 film after 1h sintering time, but did not measure the grain growth of the ZnO film. In fitting the model to the experimental data, it was assumed that both films experienced 29% grain growth after 1 h sintering time, and it was assumed that the grain growth was governed by the cubic equation, as suggested by Rahaman & De Jonghe.[11] The following grain growth equation was used for modeling the sintering of both films:

$$\frac{G}{G_0} = 1 + (0{\cdot}074)t^{1/3} \qquad (19)$$

where G_0 is the original grain size, and t is the sintering time in minutes. The kinetic parameter A was adjusted to fit the model to the data; $A = 0{\cdot}2$ for the Al_2O_3 film, and $A = 0{\cdot}08$ for the ZnO film.

Figure 5 shows the comparison of the model predictions with the data of Garino & Bowen for Al_2O_3. The experimental data shows a finite amount of shrinkage at zero time, because it accounts for the shrinkage which occurred during a 1 h hold at 1060°C, prior to sintering at 1285°C. To account for the initial shrinkage, the start time for the model was offset 5 min, as shown in the figure. Another problem with the experimental data is that for the first two data points, the linear shrinkage for the free sintering case is less than one-third the volumetric shrinkage. If the material is unconstrained and isotropic, then the shrinkage should be the same in all three coordinate directions, and the linear shrinkage will always be greater than or equal to one-third the volumetric shrinkage. This suggests that the unconstrained material was either somehow constrained, or there was some anisotropy in the material due to the processing. The model follows the trend of the data, though it does not precisely fit the data.

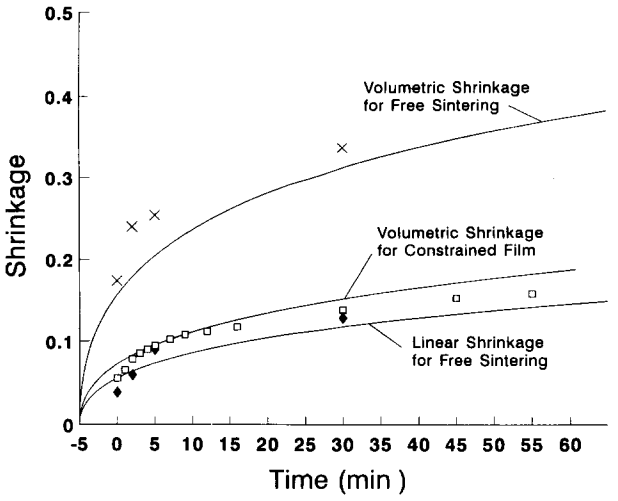

Fig. 5. Comparison of model predictions with Al_2O_3 data. ×, Volumetric shrinkage of free film; ◇, linear shrinkage of free film; □, volumetric shrinkage of constrained film.

Figure 6 shows the model fit to the ZnO data. The model follows closely with the experimental data for early sintering times, but overestimates the shrinkage for longer sintering times. The experimental data shows a decrease in the shrinkage for long sintering times, and the model can not predict a decrease in the shrinkage.

As outlined earlier the effect of grain growth

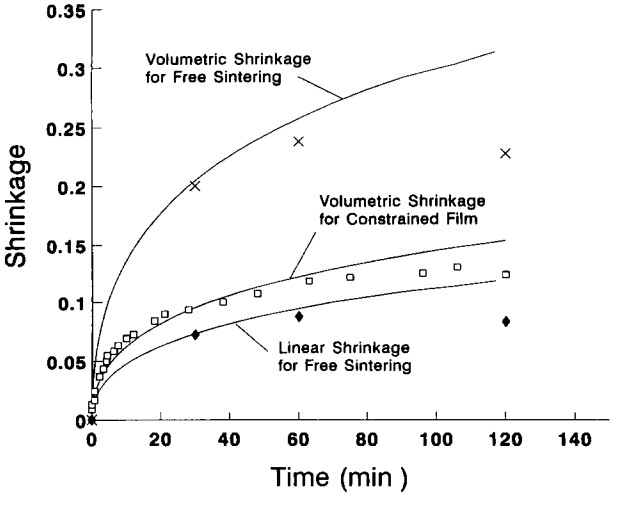

Fig. 6. Comparison of model predictions with ZnO data. ×, Volumetric shrinkage of free film; ◇, linear shrinkage of free film; □, volumetric shrinkage of constrained film

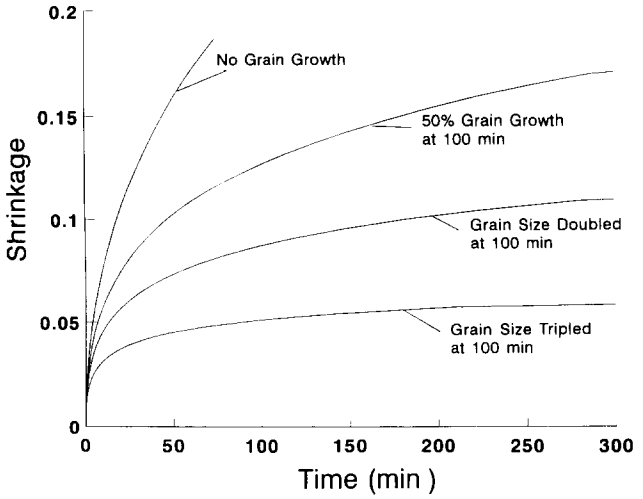

Fig. 7. Effect of grain growth on the model predictions.

can be included in the model. Figure 7 shows the effect for three different grain growth rates on the shrinkage of the film, assuming the cubic grain growth relationship. The parameters used in generating the curves were the same as used in fitting to the ZnO data by Garino & Bowen[6] except the constant (0·074) in eqn (20) was changed. The top curve shows zero grain growth, and the other three curves show a 50% increase, a doubling and a tripling in the grain size at a sintering time of 100 min. As should be expected, grain growth retards the shrinkage of the film, and large amounts of grain growth can essentially stop the shrinkage.

5 Summary and Conclusions

A physical model was developed for the initial stage of sintering of thin constrained polycrystalline films. The model assumes uniform, cubic packing of spherical particles. It provides both a qualitative and quantitative explanation for the sintering of constrained thin films. As a first approximation it was assumed that the shrinkage of a constrained thin film in the thickness direction was equal to the linear shrinkage for free sintering of the same material, and this was in reasonably good agreement with the experimental data. However, careful examination of the experimental data showed that the volumetric shrinkage of the constrained thin film was somewhat greater than the linear shrinkage for the free sintering case, and this was explained in the model by allowing material to be transported from the top and bottom necks into the side necks. The side necks act as 'material sinks', drawing material from the top and bottom necks, and increasing the shrinkage of the constrained thin film in the thickness direction.

The model shows that the densification rate of constrained thin films is highly dependent on the dihedral angle of the material and on grain growth. Small dihedral angles correspond to a low sintering pressure and a slow densification rate. Grain growth reduces the sintering pressure and increases the distances required for atomic diffusion, which further slows the densification rate. Large amounts of grain growth can essentially stop the film from densifying. The model suggests that experimental studies showing how the dihedral angle and grain growth rate of a material vary with the sintering temperature would be helpful in developing a sintering process for the material.

References

1. Scherer, G. W. & Garino, T., Viscous sintering on a rigid substrate. *J. Am. Ceram. Soc.*, **68**(4) (1985) 216–20.
2. Scherer, G. W., Sintering inhomogeneous glasses: application to optical wave guides. *J. Non-Cryst. Solids*, **34** (1979) 239–56.
3. Scherer, G. W., Sintering of low-density glasses: I. Theory. *J. Am. Ceram. Soc.*, **60**(5–6) (1977) 236–39.
4. Bordia, R. K. & Raj, R., Sintering behavior of ceramic films constrained by a rigid substrate. *J. Am. Ceram. Soc.*, **68**(6) (1985) 287–92.
5. Johnson, D. L., New method of obtaining volume, grain-boundary, and surface diffusion coefficients from sintering data. *J. Appl. Phys.*, **40**(1) (1969) 192–200.
6. Garino, T. & Bowen, H. K., Kinetics of constrained-film sintering. *J. Am. Ceram. Soc.*, **73**(2) (1990) 251–7.
7. Raj, R., Analysis of the sintering pressure. *J. Am. Ceram. Soc.*, **70**(9) (1987) C 210–C211.
8. Readey, D. W. & Jech, R. E., Energies and grooving kinetics of [001] tilt boundaries in nickel oxide *J. Am. Ceram. Soc.*, **51**(4) (1968) 201–8.
9. Handwerker, C. A., Dynys, J. M., Cannon, R. M. & Coble, R. L., Metal reference line technique for obtaining dihedral angles from surface thermal grooves. *J. Am. Ceram. Soc.*, **73**(5) (1990) 1365–70.
10. Handwerker, C. A., Dynys, J. M., Cannon, R. M. & Coble, R. L., Dihedral angles in magnesia and alumina: distribution from surface thermal grooves. *J. Am. Ceram. Soc.*, **73**(5) (1990) 1371–7.
11. Rahaman, M. N. & De Jonghe, L. C., Sintering of CdO under low applied stress. *J. Am. Ceram. Soc.*, **67**(10) (1984) C-205–C-207.